RNA secondary structures modulate hnRNPH1-mediated alternative splicing of cold-shock protein RBM3

Shuhan Shen[1], Lauren McFarlane[2,3], Marc-David Ruepp[2,3], Julie Qiaojin Lin[1]* and Deepak Khuperkar[2,3]*

[1]Bioscience and Biomedical Engineering Thrust, Systems Hub, The Hong Kong University of Science and Technology (Guangzhou), Guangzhou 511400, China
[2]UK Dementia Research Institute at King's College London, London, UK
[3]Department of Basic and Clinical Neuroscience, Institute of Psychiatry, Psychology and Neuroscience, King's College London, London, UK
*Correspondence should be addressed to qiaojinlin@hkust-gz.edu.cn and deepak.khuperkar@kcl.ac.uk

Abstract

Alternative splicing is regulated not only by sequence-specific RNA-protein interactions, but also by dynamic RNA secondary structures that remodel under varying cellular conditions. hnRNPH1, a G-rich motif-binding protein, promotes exon skipping across numerous transcripts, yet how RNA structure shapes its regulatory activity remains unclear. Building on our previous work showing that cooler temperature enhances hnRNPH1 binding to RBM3 pre-mRNA and drives poison exon (PE) skipping, we now identify RNA G-quadruplex (rG4) remodelling as the principal *cis*-acting mechanism underlying this temperature-sensitive regulation. Using small-molecule stabilizers and destabilizers, we show that rG4 folding reduces PE skipping, whereas rG4 destabilization enhances hnRNPH1-mediated PE exclusion. These effects are conserved across neuronal and non-neuronal cells. Integrating proteomics, phosphoproteomics, kinase perturbation assays, and candidates emerging from our prior genome-wide CRISPR screen, we further uncover contributions from temperature-sensitive CDC2-like kinase signalling and the RNA helicase DDX5, a known rG4 resolver and an hnRNPH1/hnRNPF co-factor. Together, our findings establish rG4 remodelling as the dominant driver of hnRNPH1-dependent RBM3 splicing, while implicating helicase activity and kinase signalling as modulatory layers that fine-tune this response. More broadly, this work illustrates how environmentally driven RNA structural transitions interface with enzymatic regulators to achieve temperature-responsive control of alternative splicing.

Keywords

Cold-shock protein, RBM3, RNA G4 structures, Alternative splicing, hnRNPH1, Poison exon, neuroprotection

Introduction

Alternative splicing (AS) is a fundamental post-transcriptional mechanism that enables a single gene to generate multiple transcript isoforms, vastly expanding the proteomic diversity of higher eukaryotes (Blencowe, 2006). This highly regulated process allows cells to dynamically respond to developmental cues, environmental stimuli such as hypothermia, and cellular stressors like hypoxia (Nilsen & Graveley, 2010; Natua et al., 2021; Neumann et al., 2020). The *trans*-acting elements of AS, primarily composed of RNA-binding proteins (RBPs) including the serine/arginine-rich (SR) proteins and heterogeneous nuclear ribonucleoproteins (hnRNPs), recognize specific RNA sequence motifs and structural elements to modulate splice site selection (Fu & Ares, 2014). Among these, hnRNPH1 binds G-rich motifs with sequence specificity and plays a crucial role in regulating exon inclusion and skipping (Caputi & Zahler, 2001; Uren et al., 2016). A key regulatory mechanism involves the inclusion of poison exons (PEs), which are short exons containing premature termination codons (PTCs) that target transcripts for nonsense-mediated mRNA decay (NMD), reducing gene expression. This mechanism has emerged as a conserved strategy for the autoregulation of splicing factors and RBPs and as a molecular switch in response to cellular stress, including temperature fluctuation (Lareau et al., 2007; Ni et al., 2007).

The cold-inducible RNA-binding motif protein 3 (RBM3) is a highly conserved RBP whose expression is robustly induced by hypothermia. As a member of the cold-shock protein family, RBM3 has been implicated in promoting mRNA stability, translation, and synaptic plasticity (Dresios et al., 2005; Peretti et al., 2015). Importantly, RBM3 confers strong neuroprotective effects in models of neurodegeneration, including Alzheimer's disease and prion disease. In these systems, RBM3 overexpression preserves synaptic function, prevents neuronal loss, and improves behavioural phenotypes, suggesting that it functions as a molecular regulator of hypothermia-induced neuroprotection (Peretti et al., 2015; Zhu et al., 2019).

We and others have shown that RBM3 expression is regulated through temperature-sensitive alternative splicing of a PE, a mechanism conserved across species and cell types (Lin, Khuperkar et al., 2023; Preußner et al., 2023). We previously identified that hnRNPH1 binds to G-rich motifs within RBM3 pre-mRNA to promote PE skipping, thereby enhancing transcript stability and RBM3 protein production at lower temperatures. Notably, hnRNPH1 shows enhanced binding to RBM3 transcripts upon cooling, indicating a temperature-responsive regulatory mechanism (Lin, Khuperkar et al., 2023).

While hnRNPH1 is a primary sequence-specific regulator of RBM3 PE splicing, several temperature-responsive features of the RNA and its regulatory environment suggest additional layers of control. The RBM3 PE contains G-rich elements capable

of forming RNA G-quadruplexes (rG4s), whose stability shifts with temperature (Zhang et al., 2025). Given hnRNPH1's known differential affinity for structured and unstructured RNA elements (Hacht et al., 2014; Haeusler et al., 2014; Neckles et al., 2019), such remodelling may dynamically modulate hnRNPH1–RNA interactions. Moreover, multiple helicases, including members of the DEAD-box family such as DDX5, can remodel rG4 structures and have been shown to cooperate with hnRNP H/F proteins in splicing regulation (Dardenne et al., 2014; Herdy et al., 2018; Wu et al., 2019). Parallel signalling mechanisms, such as phosphorylation by CDC-like kinases (CLKs), have also been implicated in cooling-responsive splice-site selection (Haltenhof et al., 2020), suggesting a broader framework in which structured RNA elements, helicase activity, and kinase signalling collectively integrate environmental temperature cues. Two non-mutually exclusive mechanisms may therefore contribute to temperature-dependent RBM3 PE regulation: 1. RNA structural remodelling, in which cooling alters rG4 folding state and thereby modulates hnRNPH1 accessibility to its binding motifs; and 2. Cooling-induced post-translational modification of hnRNPH1 or other splicing regulators, including potential phosphorylation events that may influence hnRNPH1 function or that of associated cofactors.

Here, we dissect the interplay between RNA structure, phosphorylation, and helicase biology in temperature-dependent regulation of the RBM3 poison exon. By using rG4-stabilizing and -destabilizing ligands, we directly tested the contribution of RNA structural remodelling to hnRNPH1-mediated exon definition. Through CLK inhibition and phospho-mutagenesis of hnRNPH1 RNA recognition motifs, we assessed how kinase signalling influences this process. Finally, motivated by increasing evidence that RNA helicases can remodel structured G-rich elements and cooperate with hnRNP H/F proteins, we extended our analysis to the cooling-responsive helicase DDX5, an established rG4-resolving factor and hnRNPH1 interactor. This integrated approach reveals an expanded regulatory framework linking RNA structure, helicase function, and environmental temperature to RBM3 expression.

Results:

Stabilization of rG4 structures reduces RBM3 PE skipping

We previously showed that cooling enhances hnRNPH1 binding to RBM3 pre-mRNA and promotes PE skipping, thereby stabilizing the transcript and increasing protein expression (Lin, Khuperkar et al., 2023). To investigate whether *cis*-acting RNA structures contribute to this temperature-sensitive regulation, we focused on RNA G-quadruplexes (rG4s), which are enriched in G-rich motifs within the RBM3 PE, remodel in response to temperature, and are known to influence RBP accessibility. Given hnRNPH1's preference for unstructured over structured G-rich RNA elements (Martinez-Contreras et al., 2007; Neckles et al., 2019), we reasoned that rG4 remodelling could provide a structural switch for hnRNPH1 recruitment. To test this, iPSC-derived cortical neurons (i3-neurons) were treated with the rG4 stabilizer pyridostatin (PDS), together with SMG1 inhibition to prevent nonsense-mediated

126 mRNA decay (NMD) and enable quantification of PE inclusion. RT-PCR using
127 isoform-specific primers, followed by Percent Spliced In (PSI) analysis, revealed that
128 PDS treatment significantly reduced PE skipping, indicating that stabilization of rG4
129 structures impairs the exclusion of the PE (Fig. 1A-E). This effect was conserved in
130 HeLa cells, demonstrating that rG4-mediated regulation of RBM3 splicing is not
131 limited to neurons (Fig. 1F-H). These findings are consistent with a recent study in
132 HEK cells that also reported PDS-dependent modulation of RBM3 PE splicing (Zhang
133 et al., 2025), as well as prior work showing that rG4 stabilization reduces hnRNPH1
134 binding to G-rich RNA (Khateb et al., 2007; Haeusler et al., 2014). Together, these
135 results establish that rG4 folding functions as a *cis*-acting determinant of RBM3 PE
136 regulation, likely by modulating hnRNPH1-RNA interactions.
137
138 **RBM3 PE skipping is enhanced by destabilization of rG4 structures**
139 To further assess the role of rG4 structures in RBM3 splicing regulation, i3-neurons
140 were treated with the rG4-destabilizing agent TMPyP4 (Huang et al., 2017), followed
141 by SMG1 inhibition. RT-PCR analysis demonstrated that TMPyP4 treatment led to a
142 significant increase in PE skipping, compared to control conditions (Fig. 2), consistent
143 with a model in which rG4 destabilization facilitates exon exclusion. These findings,
144 taken together with the effects of rG4 stabilization, support a model in which
145 structural remodelling of rG4 elements dynamically regulates hnRNPH1-mediated
146 RBM3 splicing.
147
148 **RBM3 PE skipping is regulated by temperature-sensitive CDC2-like kinase**
149 **(CLK)**
150 We next explored whether post-translational modifications (PTMs) contribute to the
151 differential temperature-dependent hnRNPH1-RBM3 mRNA interaction and hence
152 modulate RBM3 AS. CDC2-like kinases (CLKs) emerged as compelling candidates,
153 as they are known to phosphorylate SR proteins and modulate splicing activity in a
154 temperature-sensitive manner, with increased activity under mild hypothermia
155 (Muraki et al., 2004; Haltenhof et al., 2020). To test the functional relevance of CLK
156 activity in RBM3 splicing, we treated cells with the CLK inhibitor TG003 and assessed
157 RBM3 PE inclusion via RT-PCR. CLK inhibition led to increased PE inclusion (Fig. 3A-
158 C), implying temperature-sensitive phosphorylation events in RBM3 splicing
159 regulation. To evaluate whether hnRNPH1 is directly regulated by phosphorylation,
160 we used PhosphoSitePlus (Hornbeck et al., 2015) to predict high-confidence
161 phospho-sites. Selection was based on (a) coverage of all three RNA recognition
162 motifs (RRMs), (b) conservation between human and mouse, and (c) high
163 phosphorylation prediction scores. A panel of phospho-mutant hnRNPH1 constructs
164 was generated and tested using a previously described RBM3 minigene assay (Fig.
165 S2) (Lin, Khuperkar et al., 2023). Percent Spliced in (PSI) analyses from the RT-PCR
166 data revealed that none of the individual phospho-site mutants significantly altered
167 RBM3 PE skipping activity. These findings suggest that phosphorylation at these
168 individual residues is either not essential for splicing regulation or functionally

169 redundant across sites. Alternatively, other *trans*-acting splicing factors, such as SR
170 proteins, may serve as key phosphorylation-dependent regulators in this system.
171
172 **DDX5 is a cooling-responsive helicase linking rG4 remodelling to RBM3 PE**
173 **regulation**
174 From our analyses of RNA structure stability, we next asked whether RNA helicases,
175 which can resolve secondary structures including rG4s, participate in RBM3 PE
176 regulation. To address this, we revisited our previous genome-wide CRISPR
177 knockout screen in i3-neurons (Lin, Khuperkar et al., 2023) and identified three
178 helicases within the top 200 positive regulators of RBM3 expression: DDX58 (P =
179 0.0070, rank 102), DDX24 (P= 0.0198, rank 215), and DDX5 (P = 0.0203, rank 219)
180 (Appendix Table S3). Among these, DDX5 emerged as the most compelling
181 candidate because of the following reasons. First, multiple rG4-interactome studies
182 identify DDX5 as one of the strongest and most consistent rG4-binding and rG4-
183 resolving helicases, outperforming other DEAD-box helicases such as DDX3X and
184 DDX21 (Herdy et al., 2018). Second, DDX5 is a known physical interactor of
185 hnRNPH1/hnRNPF and cooperates with hnRNPH1/hnRNPF proteins to regulate
186 alternative splicing structures (Dardenne et al., 2014; Herdy et al., 2018; Wu et al.,
187 2019). Given this convergence, we examined whether DDX5 is temperature
188 responsive. Western blot analyses across multiple cell types—including i3-neurons,
189 HeLa and SH-SY5Y (neuroblastoma cells)—revealed a robust induction (Fold change:
190 2.19, 1.70 and 1.69-fold respectively) of DDX5 protein levels upon cooling to 32°C for
191 72 h (Fig. 4A, B, S3A). This was further supported by quantitative proteomics from
192 iPSCs revealing elevated DDX5 abundance (~1.5 fold), but not DDX17, at 32°C
193 compared to 37°C, showing that DDX5 is a cooling-responsive factor (Fig. 4C).
194 Importantly, phosphoproteomic analysis demonstrated that DDX5 phosphopeptides
195 are significantly enriched at 32 °C, mapping predominantly to RGG/RG-rich regions
196 associated with RNA structure recognition and helicase cofactor interactions,
197 indicating that DDX5 is subjected to cooling-induced post-translational modification
198 (Fig. 4D, S3B). Furthermore, kinase–substrate prediction analysis identified DDX5 as
199 a putative CLK target, with multiple phosphosite-containing peptides ranking highly
200 for CLK family kinases. Notably, two DDX5 peptides scored highest for CLK3 (Fig.
201 S3C) (Johnson et al., 2023). Because CLK inhibition increases RBM3 PE
202 inclusion (Fig. 3), these predictions provide a mechanistic link between cooling-
203 dependent kinase signalling and helicase remodelling. Collectively, these findings
204 position DDX5 as a cooling-regulated rG4-associated helicase, potentially acting
205 downstream of temperature-sensitive kinase signalling to modulate hnRNPH1-
206 dependent RBM3 splicing.
207
208 **Discussion:**
209 Our study uncovers a central role for RNA G-quadruplex (rG4) structures in regulating
210 temperature-sensitive alternative splicing of the neuroprotective cold-shock protein
211 RBM3. While we showed previously that hnRNPH1 mediates RBM3 poison exon (PE)

skipping through binding to G-rich motifs (Lin, Khuperkar et al., 2023), we now demonstrate that the RNA's structural state significantly influences this regulation. Stabilization of rG4s using pyridostatin impaired PE skipping, whereas rG4 destabilization with TMPyP4 enhanced PE exclusion, identifying rG4s as key *cis*-acting regulatory elements whose folding state influences RBM3 PE splicing.

Our findings build directly on our earlier demonstration that hnRNPH1 binding to RBM3 transcripts is enhanced upon cooling, driving PE skipping and stabilizing RBM3 mRNA (Lin, Khuperkar et al., 2023). These findings refine our earlier model by adding a structural dimension: rG4 unfolding at lower temperatures likely increases accessibility of G-rich motifs to hnRNPH1, thereby promoting PE exclusion. Although we did not directly quantify hnRNPH1-RNA binding under rG4 stabilization/ destabilization, the splicing outcomes align with hnRNPH1's established preference for unstructured G-tracts. Our results complement recent work showing that many cellular rG4s destabilize upon cooling and act as RNA thermosensors (Zhang et al., 2025). Whereas Zhang et al. highlighted transcriptome-wide consequences of rG4 remodelling, our work provides a mechanistic explanation for how rG4 dynamics translate into altered exon choice, positioning hnRNPH1 as the *trans*-acting player of this structural switch.

In addition to RNA structural changes, our data support a modulatory role for temperature-dependent post-translational modification. Inhibition of CDC2-like kinases (CLKs) increased RBM3 PE inclusion, consistent with prior evidence that CLK activity is enhanced under mild hypothermia (Haltenhof et al., 2020). However, individual phospho-site mutations in hnRNPH1 did not alter splicing outcomes (Fig. 3, S2), suggesting that phosphorylation of hnRNPH1 alone is insufficient to explain temperature-dependent regulation. This raises the possibility of combinatorial phosphorylation, redundancy among sites, or contributions from other CLK-sensitive splicing factors, such as SR proteins.

Notably, the effects of pharmacological rG4 perturbation differed depending on temperature. While rG4 stabilization by pyridostatin strongly reduced poison exon skipping at 37°C, it had no significant effect at 32°C, whereas the rG4-destabilizing ligand TMPyP4 retained a modest effect at 32°C. One possible explanation is that cooling itself induces rapid rG4 unfolding, potentially aided by increased helicase activity, such that exogenous stabilization becomes ineffective once this structural transition has occurred. These observations suggest that rG4 remodelling is an early and dominant event in the cooling response, and that additional regulatory factors may act to reinforce or sustain this unfolded state.

A major conceptual advance of the current study is the identification of DDX5 as a cooling-responsive helicase that intersects with rG4 remodelling and hnRNPH1-mediated splicing. DDX5 emerged as a positive regulator of RBM3 expression in our

prior genome-wide CRISPR knockout screen in i3-neurons (Lin, Khuperkar et al., 2023). Here, we show that DDX5 protein levels increase robustly across multiple cell types upon cooling, indicating temperature-responsive regulation. Importantly, DDX5 is a well-established rG4 resolver (Herdy et al., 2018; Wu et al., 2019) and cooperates with hnRNPH1/hnRNPF in G-rich alternative splicing programs (Dardenne et al., 2014). Phosphoproteomics further revealed multiple cooling-induced DDX5 phosphopeptides. While we could not assign these sites directly to CLK activity, DDX5 is a known substrate of SR-related kinases, supporting a model in which cooling modulates helicase function through phosphorylation. Together, these observations place DDX5 at a central intersection between RNA structural remodelling and temperature-dependent signalling, acting as an auxiliary factor that may enhance hnRNPH1 access to rG4-containing regions. Future work should determine the precise biochemical consequences of DDX5 phosphorylation on rG4 unwinding and hnRNPH1 recruitment and dissect whether DDX5 acts directly on the RBM3 rG4 itself or indirectly by remodelling nearby regulatory elements or co-factors. These studies will clarify the hierarchy and cooperativity among rG4 remodelling, helicase activity, and hnRNPH1-mediated exon definition.

Thus, RBM3 splicing appears to be governed by an integrated mechanism in which rG4 unfolding establishes the primary permissive state for hnRNPH1 activity, while DDX5 and kinase signalling fine-tune the efficiency and fidelity of this process (Fig. S4). This combinatorial interplay between RNA structure, helicase activity, and phosphorylation may represent a broader principle of temperature-responsive RNA regulation, helping ensure robust AS control under environmental perturbation.

Finally, the translational implications of our findings are substantial. RBM3 is a potent neuroprotective factor in models of Alzheimer's, prion disease, and traumatic brain injury. Our results reveal that pharmacological destabilization of rG4s enhances RBM3 expression through PE skipping, offering a potential route to mimic hypothermia-induced neuroprotection without the risks associated with therapeutic cooling. More broadly, the identification of rG4s, hnRNPH1, and DDX5 as components of a temperature-sensitive splicing axis suggests new avenues for modulating RNA structure in neurodegenerative disease.

Significance:

RNA G-quadruplexes (rG4s) are well-characterized structural elements in vitro, yet their functional impact on alternative splicing in living cells has remained unclear. Here, we show that temperature-dependent remodelling of rG4 structures within RBM3 pre-mRNA governs hnRNPH1-mediated poison exon skipping, establishing RNA structural dynamics as a primary determinant of RBM3 regulation. By integrating proteomics, phosphoproteomics, and genetic screening, we further identify the RNA helicase DDX5 as a cooling-responsive auxiliary factor which is upregulated and differentially phosphorylated at 32°C and previously shown to unwind rG4s and

cooperate with hnRNPH1 in splicing. These findings reveal how environmental cues such as mild hypothermia interface with RNA structure, helicase activity, and kinase signalling to modulate alternative splicing. More broadly, our work demonstrates a generalizable principle whereby temperature-driven RNA structural transitions help tune gene expression programs linked to cellular stress responses.

Acknowledgements:
The authors thank Jernej Ule and Flora lee (King's College London) for insightful discussions. D.K. was supported by the King's Prize Fellowship and Professor Anthony Mellows Fellowship. This research was also made possible through the support of the UK Dementia Research Institute [(UK DRI-6005 and UK DRI-6204) to M.D.R.; UK DRI Proteomics platform award (DRI-PRO2024-2) to D.K.] through UK DRI Ltd, principally funded by the Medical Research Council; the Guangdong Basic and Applied Basic Research Foundation (2023A1515111121) and the National Natural Science Foundation of China (32400453) to S.S. and J.Q.L., and Guangzhou Municipal Science and Technology Project (SL2024A04J01657) to J.Q.L.

Author Contributions
Conceptualization: J.Q.L. and D.K.; Methodology: J.Q.L., M.D.R. and D.K.; Investigation: S.S., L.M., M.D.R., J.Q.L., and D.K.; Formal analysis: S.S., J.Q.L., and D.K.; Funding acquisition: M.D.R., J.Q.L., and D.K.; Supervision and Project administration: J.Q.L. and D.K.; Visualization: S.S., J.Q.L., and D.K.; Writing-original draft: D.K.; Writing-review and editing: S.S., L.M., M.D.R., J.Q.L., and D.K.

Figure legends:

Figure 1: Stabilization of rG4 structures decreases RBM3 PE skipping. See also Figure S1

(A) Schematic of the experimental design in wildtype i3-neurons to evaluate the effect of PDS in RBM3 PE inclusion
(B) Schematic of RBM3 Exon 3a, or poison exon (PE), alternative splicing and the resulting PE-included (left) or PE-skipped (right) mRNA products. RT-PCR primer pair amplifying Exon 2–4 are indicated by grey arrows.
(C) RT-PCR of RBM3 mRNA (Exon 2–4) in i3-neurons at 37°C or 32°C (72h) in the presence of increasing concentration of PDS (0.5-1.0 μM) showing the PE-included (red arrows) and PE-skipped (green arrow) isoforms. SMG1 inhibitor (SMGi) is used to inhibit NMD.
(D) Graph showing the PSI values of RBM3 PE which are calculated based on the intensity of PE-included (red arrows) and PE-skipped (green arrow) isoforms from (C).

(E) qRT-PCR quantifying the PSI values of RBM3 PE relative to RBM3 mRNA in i3-neurons at 37°C or 32°C (72h) in the presence of increasing concentration of PDS (0.5-1.0 μM).
(F) Schematic of the experimental design in HeLa to evaluate the effect of PDS in RBM3 PE inclusion.
(G) RT-PCR of RBM3 mRNA (Exon 2–4) in HeLa at 37°C or 32°C (72h) in the presence of increasing concentration of PDS (0.5-1.0 μM) showing the PE-included (red arrows) and PE-skipped (green arrow) isoforms.
(H) qRT-PCR quantifying the PSI values of RBM3 PE relative to RBM3 mRNA in HeLa at 37°C or 32°C (72h) in the presence of increasing concentration of PDS (0.5-1.0 μM).
Data information: N = 3 biological replicates. Mean ± SEM; ns (not significant), *(P<0.05), **(P<0.01); ***(P<0.001); one-way ANOVA with multiple comparisons.

Figure 2: RBM3 PE skipping increases on destabilization of rG4 structures. See also Figure S1

(A) Schematic of the experimental design in i3-neurons to evaluate the effect of TMPyP4 in RBM3 PE inclusion
(B) RT-PCR of RBM3 mRNA (Exon 2–4) in i3-neurons at 37°C or 32°C (72h) in the presence of increasing concentration of TMPyP4 (5-200 μM) showing the PE-included (red arrows) and PE-skipped (green arrow) isoforms.
(C) Graph showing the PSI values of RBM3 PE which are calculated based on the intensity of PE-included (red arrows) and PE-skipped (green arrow) isoforms from (B).
(D) qRT-PCR quantifying the PSI values of RBM3 PE relative to RBM3 mRNA in i3-neurons at 37°C or 32°C (72h) in the presence of increasing concentration of TMPyP4 (5-200 μM).
(E) Schematic of the experimental design in HeLa to evaluate the effect of TMPyP4 in RBM3 PE inclusion (top). RT-PCR of RBM3 mRNA (Exon 2–4) in HeLa at 37°C or 32°C (72h) in the presence of increasing concentration of TMPyP4 (5-200 μM) showing the PE-included (red arrows) and PE-skipped (green arrow) isoforms (bottom).
(F) Graph showing the PSI values of RBM3 PE which are calculated based on the intensity of PE-included (red arrows) and PE-skipped (green arrow) isoforms from (E).
Data information: N = 3 biological replicates. Mean ± SEM; ns (not significant), *(P<0.05), **(P<0.01); ***(P<0.001); one-way ANOVA with multiple comparisons.

Figure 3. RBM3 PE skipping is regulated by temperature-sensitive kinase CLK. See also Figure S2

(A) Schematic of experimental procedure using CLK inhibitor (CLKi) for evaluating RBM3 PE inclusion.

(B) RT-PCR of RBM3 mRNA (Exon 2–4) in HeLa at 37°C or 32°C (72h) in the presence or absence of SMG1 inhibitor and CLK inhibitor showing the PE-included (red arrows) and PE-skipped (green arrow) isoforms.

(C) Graph showing the PSI values of RBM3 PE which are calculated based on the intensity of PE-included (red arrows) and PE-skipped (green arrow) isoforms from (B).

Data information: N = 3 biological replicates. Mean ± SEM; ns (not significant), *(P<0.05), **(P<0.01); ***(P<0.001); Unpaired t-test in (C).

Figure 4. RNA Helicase DDX5 is regulated in a cooling-dependent manner. See also Figure S3

(A) Western blot analysis of DDX5 protein levels in i3-neurons cultured at 37°C or 32°C (72h). Representative blots are shown (left) with quantification normalized to GAPDH (right).

(B) Western blot analysis of DDX5 protein levels in HeLa cultured at 37°C or 32°C (72h). Representative blots are shown (left) with quantification normalized to GAPDH (right).

(C) Global proteomics analysis from iPSCs grown at 37°C or 32°C showing significantly elevated DDX5, but not DDX17, peptide abundance under cooling conditions.

(D) Schematic showing DDX5 phosphopeptides identified from phosphoproteomics analysis. Significantly enriched peptide at 32°C is indicated in blue, with phosphorylated serine residues highlighted. Cooling-responsive phosphosites cluster within RG/RGG-rich regions implicated in RNA structure recognition.

Data information: N = 3 biological replicates. Mean ± SEM; ns (not significant), *(P<0.05), **(P<0.01); ***(P<0.001); Unpaired t-test in (A) and Welch's t-test in (B)

415 **References**

416 Blencowe, B. J. (2006). Alternative Splicing: New Insights from Global Analyses.
417 *Cell*, *126*(1), 37–47. https://doi.org/10.1016/j.cell.2006.06.023
418 Caputi, M., & Zahler, A. M. (2001). Determination of the RNA binding specificity of
419 the heterogeneous nuclear ribonucleoprotein (hnRNP) H/H'/F/2H9 family.
420 *Journal of Biological Chemistry*. https://doi.org/10.1074/jbc.M102861200
421 Dardenne, E., Polay Espinoza, M., Fattet, L., Germann, S., Lambert, M.-P., Neil, H.,
422 Zonta, E., Mortada, H., Gratadou, L., Deygas, M., Chakrama, F. Z., Samaan, S.,
423 Desmet, F.-O., Tranchevent, L.-C., Dutertre, M., Rimokh, R., Bourgeois, C. F., &
424 Auboeuf, D. (2014). RNA Helicases DDX5 and DDX17 Dynamically Orchestrate
425 Transcription, miRNA, and Splicing Programs in Cell Differentiation. *Cell*
426 *Reports*, *7*(6), 1900–1913. https://doi.org/10.1016/j.celrep.2014.05.010
427 Dresios, J., & others. (2005). Cold stress-induced protein Rbm3 binds 60S ribosomal
428 subunits, alters microRNA levels, and enhances global protein synthesis.
429 *Proceedings of the National Academy of Sciences (PNAS)*.
430 https://doi.org/10.1073/pnas.0409764102
431 Fu, X.-D., & Ares, M. Jr. (2014). Context-dependent control of alternative splicing by
432 RNA-binding proteins. *Nature Reviews Genetics*.
433 https://doi.org/10.1038/nrg3778
434 Hacht, A. von, Seifert, O., Menger, M., Schütze, T., Arora, A., Konthur, Z., Neubauer,
435 P., Wagner, A., Weise, C., & Kurreck, J. (2014). Identification and
436 characterization of RNA guanine-quadruplex binding proteins. *Nucleic Acids*
437 *Research*, *42*(10), 6630–6644. https://doi.org/10.1093/nar/gku290
438 Haeusler, A. R., Donnelly, C. J., Periz, G., Simko, E. A. J., Shaw, P. G., Kim, M.-S.,
439 Maragakis, N. J., Troncoso, J. C., Pandey, A., Sattler, R., Rothstein, J. D., &
440 Wang, J. (2014). C9orf72 nucleotide repeat structures initiate molecular
441 cascades of disease. *Nature*, *507*(7491), 195–200.
442 https://doi.org/10.1038/nature13124
443 Haltenhof, T., Kotte, A., De Bortoli, F., Schiefer, S., Meinke, S., Emmerichs, A.-K.,
444 Petermann, K. K., Timmermann, B., Imhof, P., Franz, A., Loll, B., Wahl, M. C.,
445 Preußner, M., & Heyd, F. (2020). A Conserved Kinase-Based Body-Temperature
446 Sensor Globally Controls Alternative Splicing and Gene Expression. *Molecular*
447 *Cell*, *78*(1), 57-69.e4. https://doi.org/10.1016/j.molcel.2020.01.028
448 Herdy, B., Mayer, C., Varshney, D., Marsico, G., Murat, P., Taylor, C., D'Santos, C.,
449 Tannahill, D., & Balasubramanian, S. (2018). Analysis of NRAS RNA G-
450 quadruplex binding proteins reveals DDX3X as a novel interactor of cellular G-
451 quadruplex containing transcripts. *Nucleic Acids Research*, *46*(21), 11592–
452 11604. https://doi.org/10.1093/nar/gky861
453 Hornbeck, P. V, & others. (2015). PhosphoSitePlus, 2014: mutations, PTMs and
454 recalibrations. *Nucleic Acids Research*. https://doi.org/10.1093/nar/gku1267
455 Huang, H., Zhang, J., Harvey, S. E., Hu, X., & Cheng, C. (2017). RNA G-quadruplex
456 secondary structure promotes alternative splicing via the RNA-binding protein

hnRNPF. *Genes & Development*, *31*(22), 2296–2309. https://doi.org/10.1101/gad.305862.117

Johnson, J. L., Yaron, T. M., Huntsman, E. M., Kerelsky, A., Song, J., Regev, A., Lin, T.-Y., Liberatore, K., Cizin, D. M., Cohen, B. M., Vasan, N., Ma, Y., Krismer, K., Robles, J. T., van de Kooij, B., van Vlimmeren, A. E., Andrée-Busch, N., Käufer, N. F., Dorovkov, M. V., … Cantley, L. C. (2023). An atlas of substrate specificities for the human serine/threonine kinome. *Nature*, *613*(7945), 759–766. https://doi.org/10.1038/s41586-022-05575-3

Khateb, S., Weisman-Shomer, P., Hershco-Shani, I., Ludwig, A. L., & Fry, M. (2007). The tetraplex (CGG)n destabilizing proteins hnRNP A2 and CBF-A enhance the in vivo translation of fragile X premutation mRNA. *Nucleic Acids Research*, *35*(17), 5775–5788. https://doi.org/10.1093/nar/gkm636

Lareau, L. F., & others. (2007). Unproductive splicing of SR genes associated with highly conserved and ultraconserved DNA elements. *Nature*. https://doi.org/10.1038/nature05676

Lin, J. Q., Khuperkar, D., & others. (2023). HNRNPH1 regulates the neuroprotective cold-shock protein RBM3 expression through poison exon exclusion. *EMBO Journal*. https://doi.org/10.15252/embj.2022113168

Martinez-Contreras, R., & others. (2007). hnRNP proteins and splicing control. In *Advances in Experimental Medicine and Biology*. https://doi.org/10.1007/978-0-387-77374-2_8

Muraki, M., Ohkawara, B., Hosoya, T., Onogi, H., Koizumi, J., Koizumi, T., Sumi, K., Yomoda, J., Murray, M. V., Kimura, H., Furuichi, K., Shibuya, H., Krainer, A. R., Suzuki, M., & Hagiwara, M. (2004). Manipulation of Alternative Splicing by a Newly Developed Inhibitor of Clks. *Journal of Biological Chemistry*, *279*(23), 24246–24254. https://doi.org/10.1074/jbc.M314298200

Natua, S., Ashok, C., & Shukla, S. (2021). Hypoxia-induced alternative splicing in human diseases: the pledge, the turn, and the prestige. In *Cellular and Molecular Life Sciences* (Vol. 78, Issue 6, pp. 2729–2747). Springer Science and Business Media Deutschland GmbH. https://doi.org/10.1007/s00018-020-03727-0

Neckles, C., Boer, R. E., Aboreden, N., Cross, A. M., Walker, R. L., Kim, B.-H., Kim, S., Schneekloth, J. S., & Caplen, N. J. (2019). HNRNPH1-dependent splicing of a fusion oncogene reveals a targetable RNA G-quadruplex interaction. *RNA*, *25*(12), 1731–1750. https://doi.org/10.1261/rna.072454.119

Neumann, A., & others. (2020). Alternative splicing coupled mRNA decay shapes the temperature-dependent transcriptome. *EMBO Reports*. https://doi.org/10.15252/embr.202051369

Ni, J. Z., Grate, L., Donohue, J. P., Preston, C., Nobida, N., O'Brien, G., Shiue, L., Clark, T. A., Blume, J. E., & Ares, M. (2007). Ultraconserved elements are associated with homeostatic control of splicing regulators by alternative splicing and nonsense-mediated decay. *Genes & Development*, *21*(6), 708–718. https://doi.org/10.1101/gad.1525507

Nilsen, T. W., & Graveley, B. R. (2010). Expansion of the eukaryotic proteome by alternative splicing. *Nature*. https://doi.org/10.1038/nature08909

Peretti, D., & others. (2015). RBM3 mediates structural plasticity and protective effects of cooling in neurodegeneration. *Nature*. https://doi.org/10.1038/nature14142

Preußner, M., & others. (2023). ASO targeting RBM3 temperature-controlled poison exon (paper describing ASO targeting RBM3 PE). *EMBO Molecular Medicine*. https://doi.org/10.15252/emmm.202217157

Uren, P. J., & others. (2016). High-throughput analyses of hnRNP H1 dissects its multi-functional aspect. *RNA Biology*. https://doi.org/10.1080/15476286.2015.1138030

Wu, G., Xing, Z., Tran, E. J., & Yang, D. (2019). DDX5 helicase resolves G-quadruplex and is involved in *MYC* gene transcriptional activation. *Proceedings of the National Academy of Sciences*, *116*(41), 20453–20461. https://doi.org/10.1073/pnas.1909047116

Zhang, M., Zhang, B., Liu, C., Preußner, M., Ayachit, M., Li, W., Huang, Y., Liu, D., He, Q., Emmerichs, A.-K., Meinke, S., Chen, S., Wang, L., Zheng, L., Li, Q., Huang, Q., Haltenhof, T., Gao, R., Qin, X., … Heyd, F. (2025). Stabilizing a mammalian RNA thermometer confers neuroprotection in subarachnoid hemorrhage. *Nature Communications*, *16*(1), 8319. https://doi.org/10.1038/s41467-025-63911-3

Zhu, X., & others. (2019). RBM3 promotes neurogenesis in a niche-dependent manner via IMP2-IGF2 signalling pathway after hypoxic-ischemic brain injury. *Nature Communications*. https://doi.org/10.1038/s41467-019-11870-x

Figure 1. Stabilization of rG4 structures decreases RBM3 PE skipping

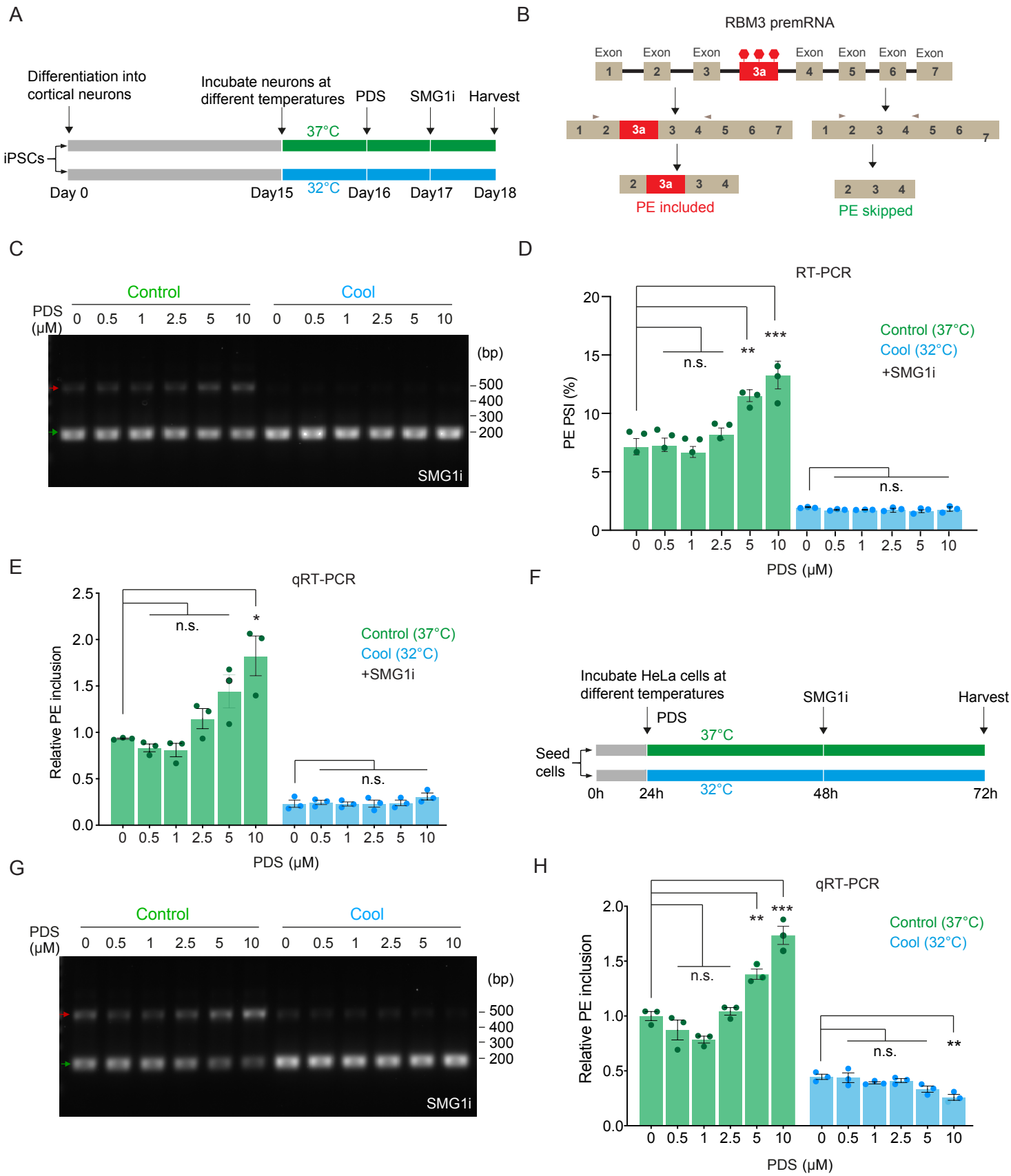

Figure 2. RBM3 PE skipping increases on destabilization of rG4 structures

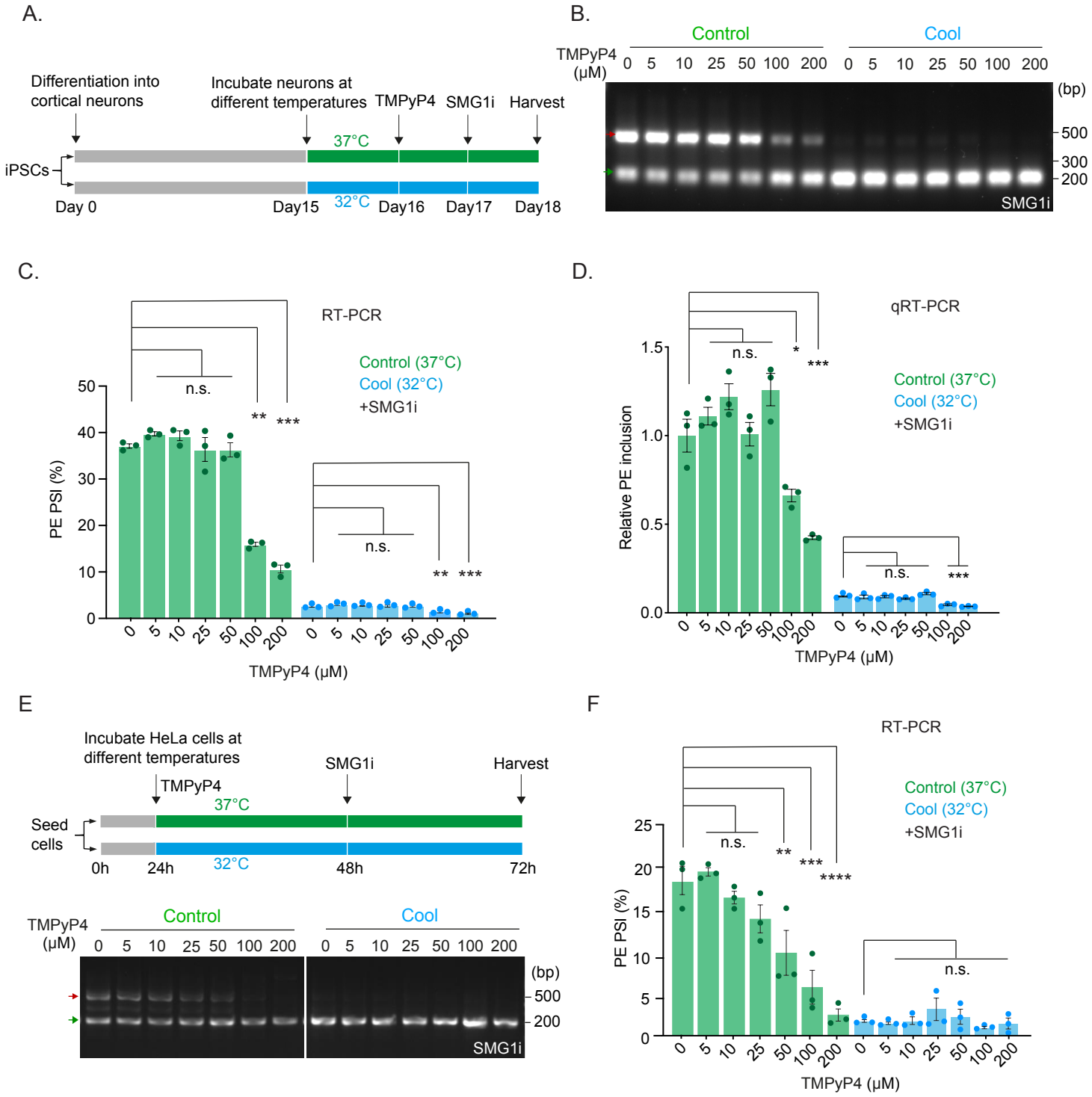

Figure 3. RBM3 PE inclusion is regulated by temperature sensitive kinase CLK

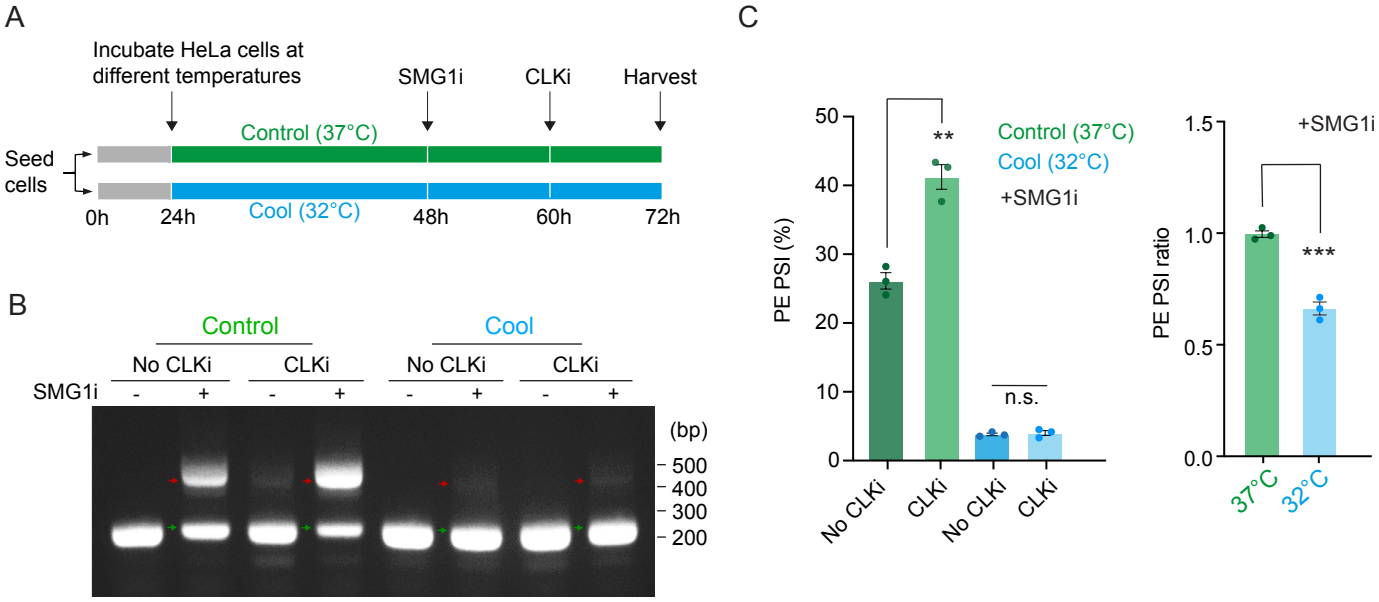

Figure 4. RNA helicase DDX5 is regulated in a cooling-dependent manner

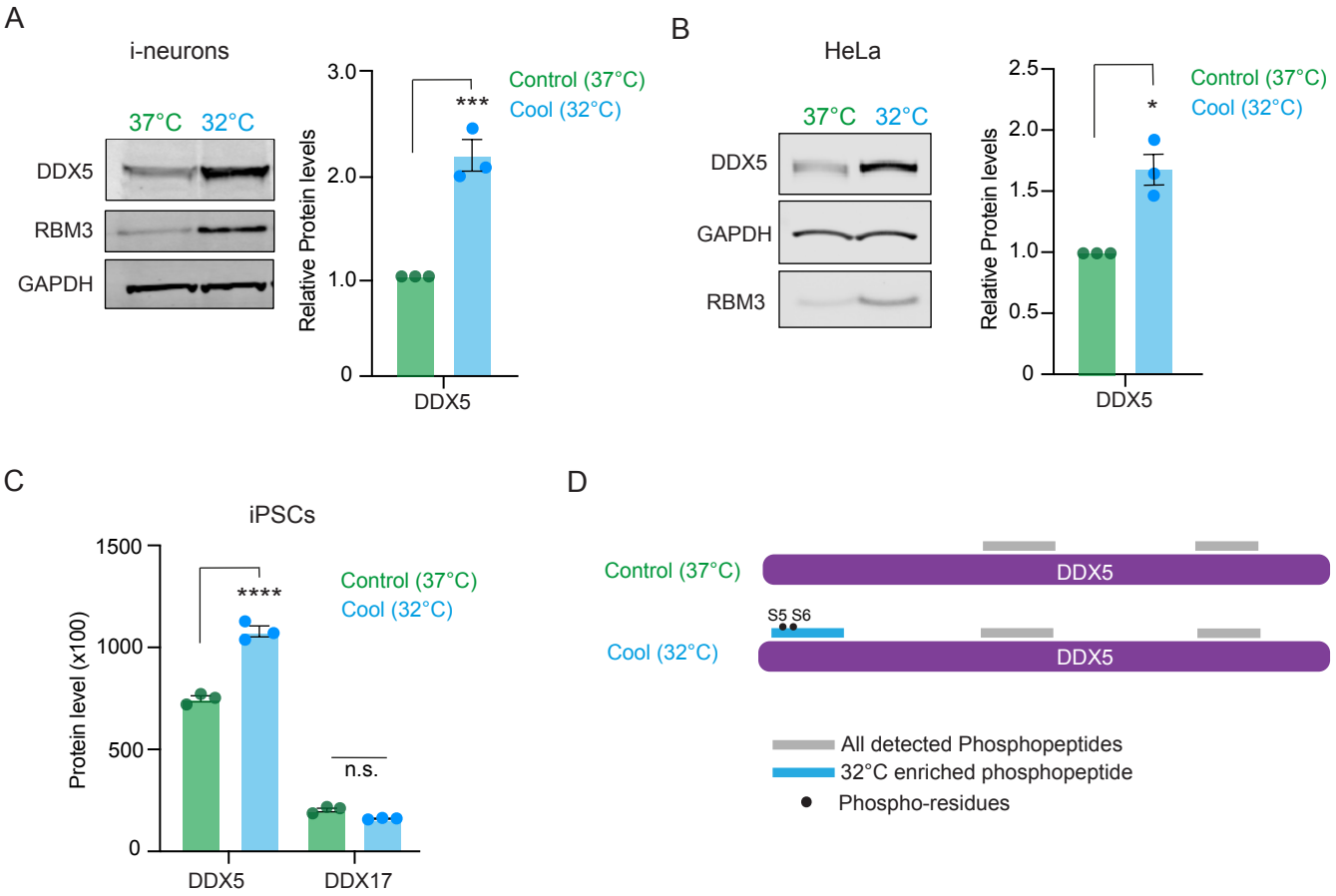

Supplementary data

Figure S1: Stability of rG4 structures influence RBM3 PE skipping

(A) Graph showing the PSI values of RBM3 PE on PDS treatment which are calculated based on the intensity of PE-included (red arrows) and PE-skipped (green arrow) isoforms from RT-PCR data in Fig. 1E.

(B) qRT-PCR quantifying the PSI values of RBM3 PE relative to RBM3 mRNA in HeLa at 37°C or 32°C (72h) in the presence of increasing concentration of TMPyP4 (5-200 μM).

Data information: N = 3 biological replicates. Mean ± SEM; ns (not significant), *(P<0.05), **(P<0.01); ***(P<0.001); one-way ANOVA with multiple comparisons.

Figure S2: Effect of hnRNPH1 phosphorylation on RBM3 PE skipping

(A) Schematic of hnRNPH1 phosphorylation sites that were targeted for phospho-dead and phospho-active mutations.

(B) Western blot from HeLa cells showing the levels of the different transfected Phosphomutants depicted in (A). GAPDH is used as loading control

(C) Schematics and RT-PCR of RBM3 minigene (Exon 1–4), flanked by unique sequences (thick black bars) to distinguish it from endogenous transcripts during PCR amplification, expressed in HeLa cells which have been co-transfected with HNRNPH1 phosphomutants, and treated with SMG1 inhibitor. The PE-included (red arrows) and PE-skipped (green arrow) isoforms are shown.

(D) Graph showing the PSI values of RBM3 PE which are calculated based on the intensity of PE-included (red arrows) and PE-skipped (green arrow) isoforms from (C)

Data information: N = 3 biological replicates. Mean ± SEM; ns (not significant), *(P<0.05), **(P<0.01); ***(P<0.001); one-way ANOVA with multiple comparisons.

Figure S3: DDX5 levels and phosphorylation increase on cooling

(A) Western blot analysis of DDX5 protein levels in SHSY-5Y (neuroblastoma) cells cultured at 37°C or 32°C (72h). Representative blots are shown (left) with quantification normalized to GAPDH (right).

(B) Summary of identified DDX5 phosphosites across cooling and control conditions from iPSCs. Phosphorylated residues and their corresponding peptides are mapped to either 37°C-specific, 32°C-specific, or shared phosphopeptide pools.

(C) Kinase-substrate prediction analyses using *The Kinase Library* for cooling-associated DDX5 phosphopeptides. Here, for two phosphosites the top 15 predicted kinases are shown, with CLK-family kinases

(CLK1/2/3/4) highlighted in blue. Multiple DDX5 phosphopeptides rank CLK enzymes among the highest-confidence motif matches, suggesting that DDX5 contains consensus sequences compatible with CLK phosphorylation.
Data information: N = 3 biological replicates. Mean ± SEM; ns (not significant), *(P<0.05), **(P<0.01); ***(P<0.001); Unpaired t-test in (A)

Figure S4: Model of rG4-dependent alternative splicing of RBM3 Poison exon

At 37°C, rG4 structures within the RBM3 PE remain folded, limiting access to hnRNPH1 and restricting PE skipping. Upon cooling to 32°C, rG4s partially unfold, enabling increased hnRNPH1 binding and promoting PE exclusion. Concurrently, DDX5 protein levels and phosphopeptide abundance increase, positioning DDX5 to cooperatively remodel rG4 or adjacent RNA structures and support hnRNPH1-mediated splicing. Predicted phosphorylation of DDX5 by CLK-family kinases provides an additional regulatory layer linking temperature-sensitive kinase activity to helicase remodelling. Together, RNA structural changes, hnRNPH1 recruitment, and DDX5 activation converge to drive enhanced RBM3 PE skipping at lower temperatures.

Supplementary Figure S1. Stability of rG4 structures affects RBM3 PE skipping

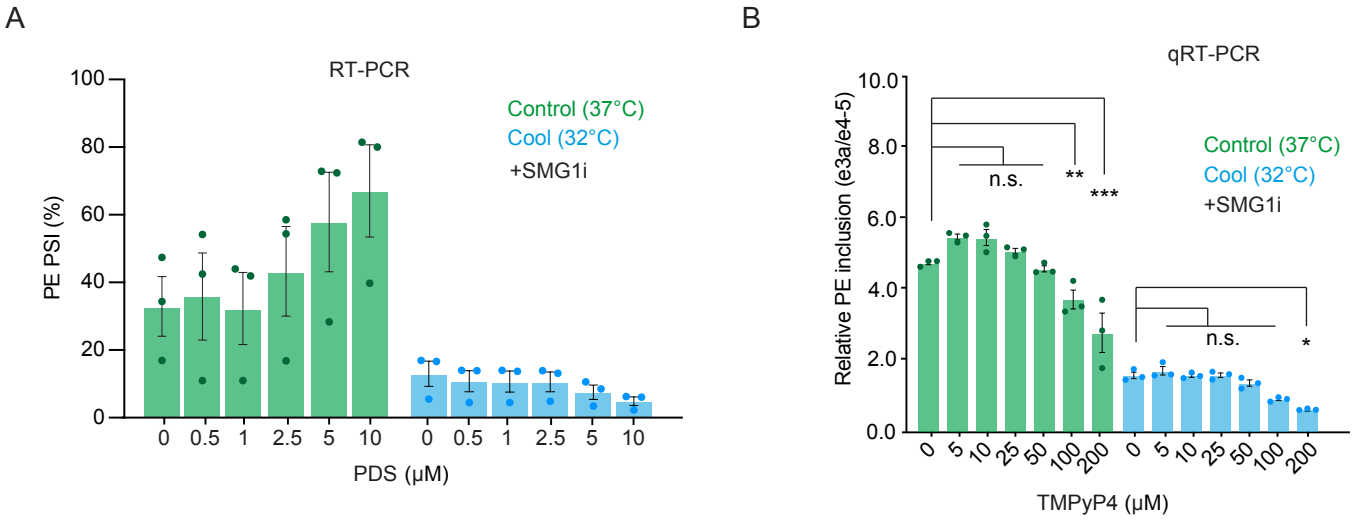

Supplementary Figure S2. Effect of HNRNPH1 phosphorylation on RBM3 PE skipping

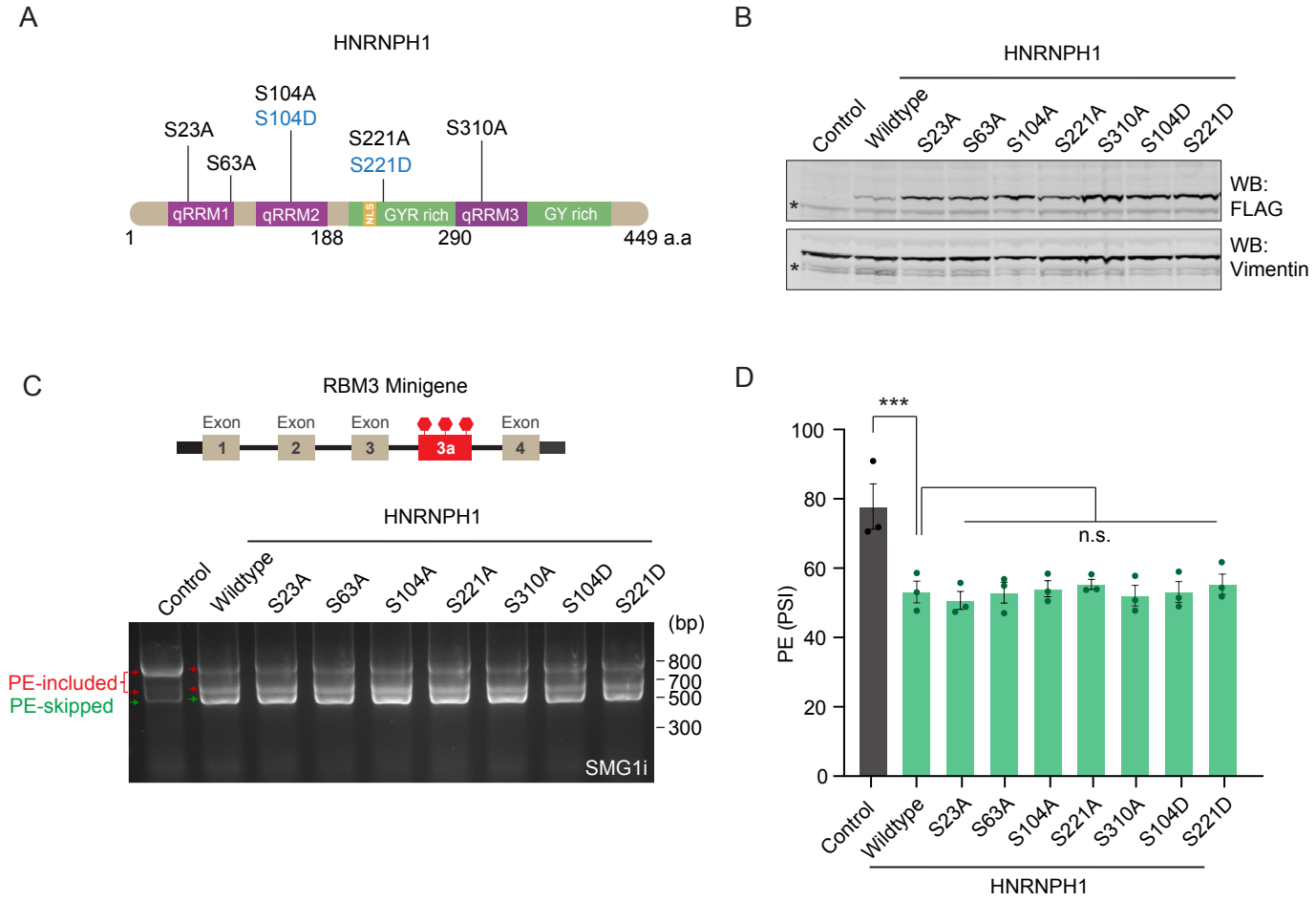

Supplementary Figure S3. DDX5 levels and phosphorylation increase on cooling

A

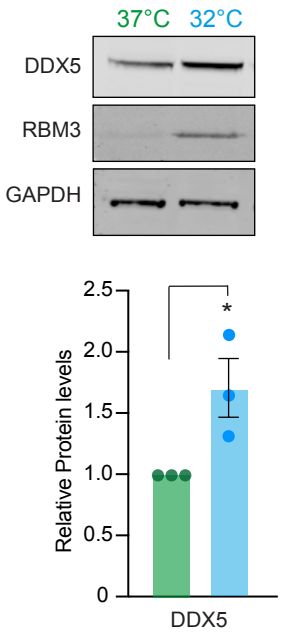

C

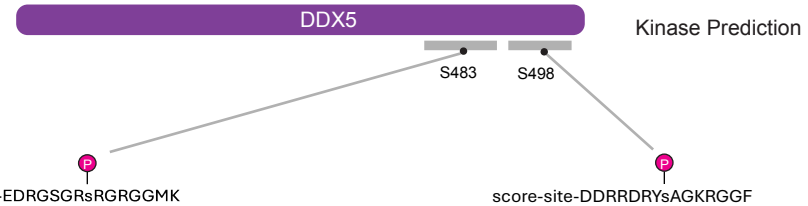

score-site-EDRGSGRsRGRGGMK

Kinase	Gene Name	Kinase Family	Log,ÇÇ(Score)	Score Rank	Site Percentile
CLK3	CLK3	CMGC	5.1495	1	99.37
SRPK1	SRPK1	CMGC	5.0808	2	98.08
CLK2	CLK2	CMGC	4.8979	3	96.29
HASPIN	HASPIN	Other	4.8797	4	99.89
WNK2	WNK2	Other	4.8329	5	99.9
SRPK2	SRPK2	CMGC	4.7697	6	98.15
IRE1	ERN1	Other	4.442	7	99.94
WNK4	WNK4	Other	4.3669	8	99.94
STK33	STK33	CAMK	4.2578	9	99.94
PKCZ	PRKCZ	AGC	4.0975	10	99.64
WNK1	WNK1	Other	4.0706	11	99.75
PKCA	PRKCA	AGC	4.0648	12	99.39
SRPK3	SRPK3	CMGC	3.9805	13	97.3
MOK	MOK	CMGC	3.7804	14	94.34
PKCI	PRKCI	AGC	3.7015	15	99.32

score-site-DDRRDRYsAGKRGGF

Kinase	Gene Name	Kinase Family	Log,ÇÇ(Score)	Score Rank	Site Percentile
CLK3	CLK3	CMGC	5.5966	1	99.61
AURC	AURKC	Other	5.1684	2	98.84
AKT2	AKT2	AGC	5.0699	3	98.7
AKT3	AKT3	AGC	5.0521	4	98.61
AURB	AURKB	Other	5.0383	5	98.94
PIM2	PIM2	CAMK	4.6763	6	98.74
AURA	AURKA	Other	4.5519	7	98.44
CLK4	CLK4	CMGC	4.4738	8	97.29
MOK	MOK	CMGC	4.3749	9	96.07
CLK2	CLK2	CMGC	4.3481	10	94.88
RSK2	RPS6KA3	AGC	4.3168	11	97.71
CLK1	CLK1	CMGC	4.1135	12	96.82
AKT1	AKT1	AGC	4.0036	13	97.67
RSK3	RPS6KA2	AGC	3.9972	14	97.8
S6K2	RPS6KB2	AGC	3.9926	15	97.91

B

Supplementary Figure S4. Model of rG4-dependent alternative splicing of RBM3 PE

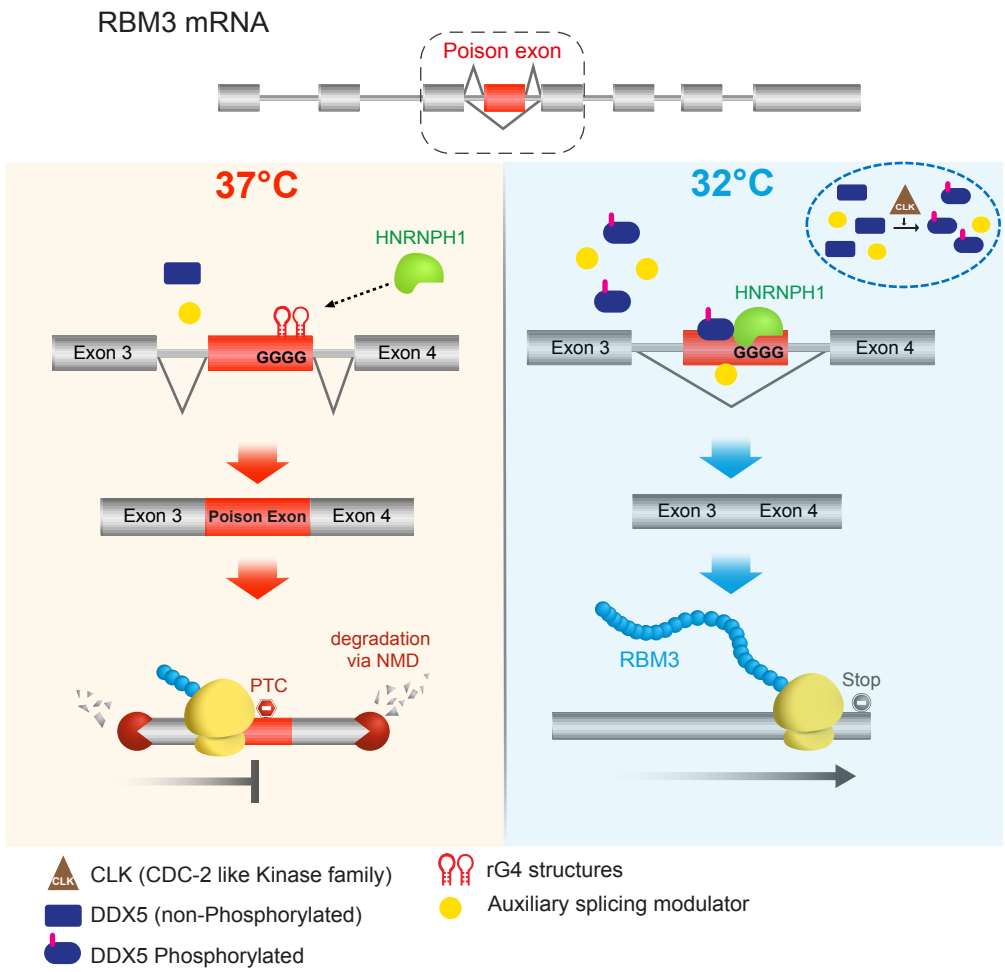

Appendix Supplementary Tables

Appendix Table S1 Primer (Pr) sequences used in this study (Page 2)
Appendix Table S2 Key resources used in this study (Page 4)
Appendix Table S3 Top three RNA Helicases from list of 220 regulators of RBM3 identified from CRISPR screen from Lin, Khuperkar et al 2023

Appendix Table S1 Primer (Pr) sequences used in this study:

Number	Name	Sequence (5' -> 3')
Pr1	qPCR_hRBM3_e3_F	GGACCTATCTCTGAGGTGGTCG
Pr2	qPCR_hRBM3_e3_R	TTCATGGCTCTCATGGCAACTG
Pr3	qPCR_hRBM3_e4-5_F	TCAGATCCGTGTGGATCATG
Pr4	qPCR_hRBM3_e4-5_R	TAATACCTGCCACTCCCATAGCC
Pr5	qPCR_hRBM3_e3a_F	GTAGTAGAGTCTGCAGACCTGTGG
Pr6	qPCR_hRBM3_e3a_R	TCCTCTAAGCTGCCCGACTATC
Pr7	hRBM3_RTPCR_fwd_DK79	GTGGGAGGGCTCAACTTTAAC
Pr8	hRBM3_RTPCR_rev_DK80	CATGATCCACACGGATCTGAC
Pr9	hRBM3_RTPCR_fwd pair 2_DK81	AGGACCGGGAGACTCAGC
Pr10	hRBM3_RTPCR_rev pair 2_DK82	AGCCACCTCCTCTGGTTC
Pr11	hRBM3_Minigene_fwd_DK20F	GCTCGGATCCACTAGTCCAGTGT
Pr12	hRBM3_Minigene_rev_DK21R	GTTTAAACGGGCCCTCTAGACT
Pr13	hRBM3 qPCR ex2_fwd_DK30	TCAGCAGTTTCGGACCTATC
Pr14	hRBM3 qPCR ex3_rev_DK31	CATGCTCTGGGTTGGTGAAG
Pr15	GAPDH qpCR_fwd	CCAGAACATCATCCCTGCCT
Pr16	GAPDH qpCR_rev	GGTCAGGTCCACCACTGACA
Pr17	qPCR_h18S_F	GTAACCCGTTGAACCCCATT

Pr18	qPCR_h18S_R	CCATCCAATCGGTAGTAGCG
Pr19	HNRNPH1 S23A_f	ACCTCATCGGCAGCACAGGACCAGGGC
Pr20	HNRNPH1 S23A_r	GCCCTGGTCCTGTGCTGCCGATGAGGT
Pr21	HNRNPH1 S63A_f	CACTTCGTCCTCGGCTTCCAGTTCCACAAAGGCTTC
Pr22	HNRNPH1 S63A_r	GAAGCCTTTGTGGAACTGGAAGCCGAGGACGAAGTG
Pr23	HNRNPH1 S104A_f	GGCTGTGTCGGGGGCGTTAGGGCCTGTGT
Pr24	HNRNPH1 S104A_r	ACACAGGCCCTAACGCCCCCGACACAGCC
Pr25	HNRNPH1 S104D_f	TGGCTGTGTCGGGGTCGTTAGGGCCTGTGTG
Pr26	HNRNPH1 S104D_r	CACACAGGCCCTAACGACCCCGACACAGCCA
Pr27	HNRNPH1 S221A_f	CGCCTCTTCCGATAGCGTTGTAGCCTCTGCC
Pr28	HNRNPH1 S221A_r	GGCAGAGGCTACAACGCTATCGGAAGAGGCG-
Pr29	HNRNPH1 S221D_f	GGCGCCTCTTCCGATATCGTTGTAGCCTCTGCCA
Pr30	HNRNPH1 S221D_r	TGGCAGAGGCTACAACGATATCGGAAGAGGCGCC
Pr31	HNRNPH1 S310A_f	CACGGGGTTCAGAGGGGCGAAGAAATTGTAGATGTCGTT
Pr32	HNRNPH1 S310A_r	AACGACATCTACAATTTCTTCGCCCCTCTGAACCCCGTG

Appendix Table S2 Key resources used in this study:

REAGENT or RESOURCE	SOURCE	IDENTIFIER
Antibodies		
Mouse anti-FLAG antibody	Sigma	Cat#F1804
Rabbit anti-RBM3 antibody	Proteintech	Cat#14363-1-AP
Mouse anti-GAPDH antibody	Santa Cruz Biotechnology	Cat#sc-32233
Rabbit anti-Vimentin antibody	Santa Cruz Biotechnology	Cat#sc5565
Rabbit anti-DDX5 antibody	Proteintech	Cat#26385-1-AP
Donkey anti-rabbit 680LT	LI-COR	Cat#926-68023
Donkey anti-mouse 680LT	LI-COR	Cat#926-68022
Donkey anti-mouse 800CW	LI-COR	Cat#926-32212
Donkey anti-rabbit 800CW	LI-COR	Cat#926-32213
Bacterial and virus strains		
One Shot™ Stbl3™ chemically competent *E. coli*	Thermo Fisher Scientific	Cat#C737303
XL10-Gold Ultra-competent	Agilent Technologies	Cat#50-125-094
Chemicals, peptides, and recombinant proteins		
TeSR-E8 Medium	Stemcell Technologies	Cat#05990
mTeSR™ Plus	Stemcell Technologies	Catalog#100-0276
StemFlex Medium	Thermo Fisher Scientific	Cat#A3349401
EDTA, pH8.0	Thermo Fisher Scientific	Cat#15575020
Vitronectin	Thermo Fisher Scientific	Cat#A14700
Cryostor Cs10 Cryopreservation	Merck	Cat#C2874-100ML

StemPro Accutase Cell Dissociation Reagent	ThermoFisher Scientific	Cat#A1110501
0.25% Trypsin-EDTA	Merck	Cat#T4049
Rho-associated protein kinase (ROCK) inhibitor	BD Biosciences	Cat#Y-27632
Geltrex LDEV-Free, hESC-Qualified, Reduced Growth	Life Technologies	Cat#A1413302
DMEM/F12, GlutaMAX Supplement	Thermo Fisher Scientific	Cat#31331028
DMEM, high glucose, GlutaMAX™ Supplement	Gibco	Cat#10566016
Fetal Bovine Serum	Sigma	Cat# F0193
N-2 Supplement (100X)	Thermo Fisher Scientific	Cat#17502048
MEM Non-Essential Amino Acids Solution (100X)	Thermo Fisher Scientific	Cat# 11140050
2-Mercaptoethanol (50 mM)	Thermo Fisher Scientific	Cat#31350010
Doxycycline hyclate	Merck	Cat#D9891
Neurobasal medium	Thermo Fisher Scientific	Cat#21103049
Neurobasal medium, minus phenol red	Thermo Fisher Scientific	Cat#12348017
B-27 Supplement (50X), minus vitamin A	Thermo Fisher Scientific	Cat#12587010
GlutaMAX Supplement	Thermo Fisher Scientific	Cat# 35050061
Neurotrophin-3 (NT-3)	PeproTech	Cat#450-03
Brain Derived Neurotrophic Factor (BDNF)	PeproTech	Cat#450-02
Penicillin-Streptomycin	Thermo Fisher Scientific	Cat#15140122
Proteinase K, recombinant, PCR grade	Thermo Fisher Scientific	Cat#EO0491
Sodium Acetate, 3M, pH 5.2	Merck	Cat#567422-100ML
Poly-L-lysine	Merck	Cat#P4707
Laminin	Merck	Cat#L2020-1MG
Tween-20	Merck	Cat#P9416-50ML

RIPA buffer	Merck	Cat#R0278-500ML
DNase 1	Zymo	Cat#E1011-A
HALT protease inhibitor cocktail	Thermo Fisher Scientific	Cat#1861278
TRIzol	Invitrogen	Cat#15596018
HALT protease and phosphatase inhibitor cocktail	Thermo Fisher Scientific	Cat#78442
cOmplete, EDTA-free Protease Inhibitor Cocktail	Merck/Roche	Cat#11873580001
SMG1 inhibitor	ProbeChem	Cat#PC-35788
Pyridostatin hydrochloride	Merck	Cat#SML2690-5MG
TMPyP4	Merck-Sigma	Cat# 613560
CLK inhibitor (TG003)	Apexbio	Cat#B1431-APE-5mg
RIPA buffer	Beyotime	Cat#PO013B
Protease inhibitor cocktail	Roche	Cat#4693132001
Phosphatase inhibitor cocktail II	MCE	Cat#HY-K0022
Phosphatase inhibitor cocktail III	MCE	Cat#HY-K0023
Acetone	Guangzhou	Cat#HPLC500-008
Urea	Sigma	Cat#51456
1M Tris-HCl (pH 8.5)	Beyotime	Cat#ST785
TCEP	Macklin	Cat#T917415
Iodoacetamide	Sigma	Cat#I1149-5g
Calcium chloride	Sigma	Cat#C1016-100G
Methylamine	Aladdin	Cat#M102702-100ml
Trypsin	Promega	Cat#V5111
Formic acid	Merck	Cat#F0507

Acetonitrile	Merck	Cat#34851
Methanol	Macklin	Cat#M813903
Acetic acid	Sigma	Cat#5.33001
Critical commercial assays		
Absolutely RNA Minprep Kit	Agilent	Cat#400800
FastPure® Cell/Tissue Total RNA Isolation Kit V2	Vazyme	Cat# RC112-01
SuperScript IV First-Strand Synthesis System	Thermo Fisher Scientific	Cat#18091050
Q5 High-Fidelity DNA Polymerase	NEB	Cat#M0492L
TB Green® Premix Ex Taq™	Takara	Cat# RR820A
NEBuilder HiFi DNA Assembly Master Mix	NEB	Cat#E2621L
GoTaq Taq G2 Green Master Mix	Promega	Cat#M7823
BCA Protein Assay Kit	Thermo Fisher Scientific	Cat#23225
PrimeSTAR Max DNA Polymerase Mix	Takara	Cat# R047A
TransIT-LT1	Mirus	Cat#22043217
dNTP Mix	Thermo Fisher Scientific	Cat#R0192
RiboLock RNAse inhibitor	Thermo Fisher Scientific	Cat#EO0381
AffinityScript Multi temperature Multiple Reverse Transcriptase	Agilent	Cat#600107-51
PrimeScript™ RT Reagent Kit	Takara	Cat# RR047A
AffinityScript RT buffer	Agilent	Cat#600100-52
DTT	Agilent	Cat#600100-53
QuickChange Lightning Multi Site-Directed Mutagenesis Kit	Agilent	Cat#210513
High-Select™ TiO_2 Phosphopeptide Enrichment Kit	Thermo Fisher Scientific	Cat#A32993

Experimental models: Cell lines		
Human iPSC/iPSC-derived neuron: Bob (wild-type)	(Lin, Khuperkar et al., 2023)	N/A
HeLa	ECACC	Cat#93021013
Oligonucleotides		
Primers used in this study are listed in Table S1	This study	N/A
Recombinant DNA		
Plasmid: RBM3 Minigene	(Lin, Khuperkar et al., 2023)	N/A
Plasmid: HNRNPH1-WT	(Lin, Khuperkar et al., 2023)	N/A
Plasmid: HNRNPH1-S23A	This study	N/A
Plasmid: HNRNPH1-S63A	This study	N/A
Plasmid: HNRNPH1-S104A	This study	N/A
Plasmid: HNRNPH1-S104D	This study	N/A
Plasmid: HNRNPH1-S221A	This study	N/A
Plasmid: HNRNPH1-S221D	This study	N/A
Plasmid: HNRNPH1-S310A	This study	N/A
Software and algorithms		
Prism (v10.6.2)	GraphPad	https://www.graphpad.com
FIJI (v2.1.0)	(Schindelin et al., 2012)	https://fiji.sc/
Design and Analysis Software (v2.6.0)	Thermo Fisher Scientific	N/A
PEAKS® Studio 13	Bioinformatics Solutions Inc.	https://www.bioinfor.com/peaks-studio/
Spectronaut®	BIOGNOSYS	https://biognosys.com/software/spectronaut/

Appendix Table S3 Top three RNA Helicases from list of 220 regulators of RBM3 identified from CRISPR screen from Lin, Khuperkar et al 2023

id	Gene symbol	Full gene name	neg|p-value	neg|rank	neg|lfc	pos|p-value	pos|rank
ENSG00000107201	DDX58	DExD/H-box helicase 58(DDX58)	**0.0070304**	102	-0.28976	**0.042293**	2476
ENSG00000089737	DDX24	DEAD-box helicase 24(DDX24)	**0.019821**	215	-0.28775	**0.052726**	2968
ENSG00000108654	DDX5	microRNA 3064(MIR3064)	**0.020337**	219	-0.39733	**0.73672**	15690

References

Lin, J. Q., Khuperkar, D., & others. (2023). HNRNPH1 regulates the neuroprotective cold-shock protein RBM3 expression through poison exon exclusion. *EMBO Journal*. https://doi.org/10.15252/embj.2022113168

Schindelin, J., Arganda-Carreras, I., Frise, E., Kaynig, V., Longair, M., Pietzsch, T., Preibisch, S., Rueden, C., Saalfeld, S., Schmid, B., Tinevez, J.-Y., White, D. J., Hartenstein, V., Eliceiri, K., Tomancak, P., & Cardona, A. (2012). Fiji: an open-source platform for biological-image analysis. *Nature Methods*, *9*(7), 676–682. https://doi.org/10.1038/nmeth.2019

Material Methods

Plasmids and oligonucleotides

All primers used in this study are listed in Appendix Table S1. Plasmids generated alongside key resources are listed in Appendix Table S2.

HNRNPH1 phosphomutants: FLAG-HNRNPH1 phosphomutants were generated using site directed mutagenesis (QuickChange Lightning Multi Site-Directed Mutagenesis Kit, Agilent) from FLAG-HNRNPH1 plasmid (described previously in Lin, Khuperkar et al., 2023) using specific primers (See Table S1). Sequences within the promoter and insert regions were confirmed by Sanger sequencing.

HeLa cell culture and transfection

HeLa cells were grown in Dulbecco's Modified Eagle Medium (DMEM, high glucose, GlutaMAX™ Supplement; Gibco) supplemented with 10% fetal bovine serum (Sigma) or Dulbecco's modified Eagle's medium (DMEM)+ Ham's F12 (1:1) supplemented with 10% fetal calf serum (FCS), penicillin (100 IU/mL), and streptomycin (100 µg/mL) at 37°C under 5% CO_2. Plasmid DNA transfection was performed with TransIT-LT1 (Mirus) according to the manufacturer's instructions. For HNRNPH1 overexpression experiments, 250,000 HeLa cells were seeded in a 6-well plate, and the next day cells were co-transfected with HNRNPH1 constructs and RBM3 Minigene (described previously in Lin, Khuperkar et al., 2023). After 24h, medium was changed again with fresh medium with or without 1 µM SMG1 inhibitor (Probechem, PC-35788). Cells were incubated with SMG1 inhibitor for 24h before harvesting the cells.

Human iPSC culture and differentiation into iPSC-derived neurons (i3-neurons)

Human iPSCs with Neurogenin-2 (NGN2) transgene stably integrated into a 'safe-harbour' locus under doxycycline (Dox)-inducible promoter (described previously in Lin, Khuperkar et al., 2023) were maintained under feeder-free conditions in TeSR-E8 medium in a 37°C, 5% CO_2 tissue culture incubator. They were cultured on vitronectin (3.3 µg/mL)-coated culture plates or glass-bottom dishes and fed every day with TeSR-E8 medium or every 2 days with StemFlex Medium. 0.5 mM EDTA was used for routine dissociation to maintain colony growth.

iPSCs were enzymatically detached and dissociated into single cells using Accutase and plated into GelTrex (1:100 dilution)-coated culture plates in TeSR-E8 medium supplemented with 10 µM Rho-associated protein kinase (ROCK) inhibitor. After 24 hours (day 1), TeSR-E8 medium was changed to DMEM/F12 medium with GlutaMAX, supplemented with 1x N-2 supplement, 1x Non-Essential Amino Acids, 50 nM 2-Mercaptoethanol, 100 U/mL Penicillin-Streptomycin, and 1 µg/mL Doxycycline Hyclate (Dox) (iN-1 medium). After 24 hours (day 2), the medium was replaced with the same medium as the previous day. From day 3 to day 6, the culture was fed daily with Neurobasal medium supplemented with 1x B-27 supplement (minus vitamin A), 1x GlutaMAX, 50 nM 2-Mercaptoethanol, 100 U/mL Penicillin-Streptomycin, and 1

μg/mL Dox, 10 ng/mL Neurotrophin-3 (NT-3), and 10 ng/mL Brain-derived neurotrophic factor (BDNF) (iN-2 medium). After day 6, the medium was changed every other day. The same feeding schedule as previously described was followed from day 5. I-neurons in the 32°C conditions were placed in a 5% CO_2 incubator set to 32°C for 72h between day 15-18 post differentiation. For PE analyses, neurons were incubated with SMG1 inhibitor for 24h before collection.

Drug treatments

PDS: HeLa cells were seeded and grown at 37°C. 24h post seeding, one set of cells was incubated at 32°C, while the other remained at 37°C. After 24h, the medium was replaced with fresh medium containing PDS (Merck-Sigma) at different concentrations (0, 0.5, 1, 2.5, 5 or 10 μM). Following another 24h incubation, the SMG1 inhibitor was added to a final concentration of 1 μM, and cells were harvested after an additional 24h. For i3-neurons, on day 15 post differentiation, one set of the i3-neurons was incubated at 32°C, while the other remained at 37°C. This was followed by PDS treatment with the same concentration range as described above on Day 16 (after 24h), SMG1 inhibitor incubation (1 μM) on Day 17 and harvesting on Day 18 post differentiation.

TMPYP4: HeLa cells were seeded and grown at 37°C. 24h post seeding, one set of cells was incubated at 32°C, while the other remained at 37°C. After 24h, the medium was replaced with fresh medium containing TMPyP4 (Merck-Sigma) at different concentrations (0, 5, 10, 25, 50, 100, or 200 nM). Following another 24h incubation, the SMG1 inhibitor was added to a final concentration of 1 μM, and cells were harvested after an additional 24h. For i3-neurons, on day 15 post differentiation, one set of the i3-neurons was changed to 32°C, while the other remained at 37°C. This was followed by TMPyP4 treatment with the same concentration range as described above on Day 16 (after 24h), SMG1 inhibitor incubation (1 μM) on Day 17 and harvesting on Day 18 post differentiation.

CLK inhibitor (TG003): HeLa cells were seeded and grown at 37°C. 24 hours later, one set of cells was incubated at 32°C, while the other remained at 37°C. After 24h, the medium was replaced with fresh medium containing CLK inhibitor (TG003) (Apexbio) at 10μM. Following another 24h incubation, the SMG1 inhibitor was added to a final concentration of 1 μM, and cells were harvested after an additional 24h for RNA extraction.

RT-PCR and qRT-PCR

Total RNA of i3-neurons and HeLa cells was extracted using the Absolute RNA miniprep kit or the FastPure®Cell/Tissue Total RNA Isolation Kit V2 (Vazyme). Reverse transcription to generate cDNA was performed using the PrimeScript™ RT Reagent Kit (Takara) or AffinityScript Multiple Temperature Reverse Transcriptase. When using the latter method, 1-2 μg of isolated RNA was incubated with random

hexamers (900ng) in a total volume of 67 µl in DEPC water at 65°C for 5 minutes and then for 10 minutes at room temperature. Then, the mixtures were separated into 2 parts – RT and no-RT control samples (33.5 µl each). To this 13.5 µl master mix was added to supplement 1x reverse transcriptase buffer (Agilent), 10 mM DTT (Agilent), 400 µM dNTPs (Thermo Scientific), 40 units RiboLock RNase inhibitor (Thermo Scientific) and 1 reaction equivalent AffinityScript Multiple Temperature Reverse Transcriptase (Agilent). The RT enzyme was absent in the no-RT condition. The samples were then incubated at 65°C for 1 hour followed by heat-inactivation at 75°C for 20 minutes.

For RT-PCR, 20-40 ng cDNA was amplified using GoTaq Polymerase mix or the PrimeSTAR Max DNA Polymerase Mix (Takara) using the indicated primers (Appendix Table S1). Quantification of the bands on agarose gels was done using FIJI software. Percent spliced in (PSI) indexes of RBM3 poison exon (PE) are calculated based on the intensity of PE-included (red arrows) and PE-skipped (green arrows) isoforms visualised in agarose gels:

a) One PE-included isoform is detected: $(I_{Inc}/L_{Inc}) / (I_{Inc}/L_{Inc} + I_{skip}/L_{skip})$, or
b) Two PE-included isoforms are detected: $(I_{Inc1}/L_{Inc1} + I_{Inc2}/L_{Inc2}) / (I_{Inc1}/L_{Inc1} + I_{Inc2}/L_{Inc2} + I_{skip}/L_{skip})$

Where I_{Inc} = Intensity of PE-included isoform, L_{Inc} = length of PE-included isoform in base pairs, I_{Inc} = Intensity of PE-skipped isoform, L_{skip} = length of PE-skipped isoform in base pairs.

For qRT-PCR, cDNA from each sample (diluted 10–1,000-fold) was mixed with TB Green® Premix Ex Taq™ (Takara) and PCR primers in four technical replicates on 384-well plates. Reactions were run on a LightCycler® 480 Instrument II (Roche), and data were analyzed using LightCycler 480 software (Roche). Relative PE inclusion was calculated as the ratio of the RBM3 Exon 3a amplicon to either the RBM3 Exon 3 or Exon 4–5 amplicon (or their geometric mean). 18S rRNA served as the loading control for quantifying RBM3 and HNRNPH1 mRNA levels.

Cell lysis and Western blotting

HeLa cells were harvested by scraping and washed with 1x Phosphate buffered saline (PBS). Lysis was done in 150 µl RIPA lysis buffer (Merck) per well of 6-wells plate, supplemented with 1x Halt Protease Inhibitor cocktail (Thermo Scientific), followed by sonication at 40% amplitude on ice. The extracts were then cleared by centrifugation at 15,000 x g and 4°C for 15 minutes. Protein concentrations of lysates were determined by BCA assay following the manufacturer's instruction. Samples were diluted with Laemmli protein sample buffer with 100 mM DTT. 20 µg protein was loaded into each well on a 4–12% Bis-Tris polyacrylamide gels (NuPAGE) followed by western blotting and ran at 150 V. Gels were dry blotted onto nitrocellulose

membranes on an iBlot2 gel transfer system (Invitrogen). Membranes were blocked with 5% non-fat milk in 1x TBS-T for 1 h rotating at room temperature. The primary antibody solution was incubated overnight at 4°C while rotating. The next day, membranes were washed three times with 1x TBS-T, then incubated for 1 h in secondary antibody solution (1:10,000 in 5% non-fat milk in 1x TBS-T) and washed three times with 1x TBS-T before imaging on LI-COR Odyssey CLx. Primary and secondary antibodies were used in the following concentrations: Rabbit anti-RBM3 (1:1500), mouse anti-GAPDH (1:3000), Rabbit anti-DDX5 (1:3000), Rabbit anti-Vimentin (1:2000), mouse anti-FLAG (1:3000), donkey anti-mouse 680LT (1:10000), donkey anti-rabbit 800CW (1:10000) and donkey anti-mouse 800CW (1:10000).

hnRNPH1 phosphosites prediction

Putative phosphorylation sites within full-length human HNRNPH1 (UniProt ID: Q00464) were identified using the PhosphoSitePlus database (Hornbeck et al., 2015). Candidate residues were shortlisted according to the following criteria: (i) distribution across all three RNA recognition motifs (RRMs) to ensure domain-wide coverage, (ii) evolutionary conservation between human and mouse sequences, and (iii) high-confidence phosphorylation scores reported in the database. Sites fulfilling these criteria were selected for subsequent site-directed mutagenesis to generate phospho-deficient (serine to alanine) and phospho-mimetic (serine to aspartate) hnRNPH1 constructs for functional assays.

Total proteomics and Phospho-proteomics

The lysis buffer, composed of RIPA (Beyotime) supplemented with 1X protease inhibitor cocktail (Roche), 1X phosphatase inhibitor cocktail II (MCE), and 1X phosphatase inhibitor cocktail III (MCE), was directly added to the culture dish of iPSC cells. Prior to lysis, the cells were washed once with 1× Dulbecco's phosphate-buffered saline (DPBS). The cells were then harvested using a cell scraper. The resulting cell lysate was transferred to a centrifuge tube. Four volumes of pre-chilled acetone (-20°C) were added to the lysate, followed by vortexing and incubation at -20°C overnight. After incubation, the sample was centrifuged at 12,000 × g and 4°C for 10 minutes. The supernatant was discarded, and the pellet was washed once with a fresh volume of pre-chilled acetone. The pellet was then air-dried in a biosafety cabinet with the tube lids open at room temperature to evaporate residual acetone. The proteins were solubilized in a freshly prepared solution of 8M urea (Sigma) and 100 mM Tris (pH 8.5) (Beyotime). Protein concentration after precipitation was determined by a BCA assay (Thermo) to guide subsequent trypsin usage. For reduction, TCEP (Macklin) was added to a final concentration of 5 mM, and the sample was incubated at room temperature for 20 minutes. This was followed by alkylation through the addition of iodoacetamide (Sigma) to a final concentration of 10 mM, with incubation in the dark at room temperature for 15 minutes. The sample was then diluted four-fold with 100 mM Tris (pH 8.5) to reduce the urea concentration.

$CaCl_2$ was added to a final concentration of 1 mM, and methylamine was added to 20 mM to minimize carbamylation. Trypsin (Promega) was added at a 1:100 (w/w) enzyme-to-protein ratio. Digestion was carried out in the dark at 37°C overnight (~16 h). The tryptic digestion was stopped by acidifying the sample with formic acid (Merck) to a final concentration of 0.5%. For desalting, a large C18 column (Waters) was used. The column was conditioned with 1 mL of methanol, washed with 1 mL of 80% acetonitrile (Merck) (in 0.5% acetic acid (Sigma)), and equilibrated with 1 mL of 0.5% acetic acid. The acidified sample was loaded onto the column, which was then washed three times with 1 mL of 0.5% acetic acid. Peptides were eluted by applying 500 μL of 80% acetonitrile, and the same eluent was passed through the column a second time into the same tube. The peptide eluate was dried in a SpeedVac vacuum concentrator at 35°C for approximately 2h. The resulting peptide powder was stored at -80°C. The peptide sample was subsequently split: one portion was used for total proteome analysis, and the other portion was subjected to phosphopeptide enrichment using the High-Select™ TiO2 Phosphopeptide Enrichment Kit (Thermo Fisher Scientific) according to the manufacturer's instructions. Prior to LC-MS/MS analysis, the peptides were reconstituted in 0.1% formic acid. All LC-MS/MS analyses were performed on a timsTOF HT mass spectrometer coupled with a nanoElute 2 HPLC system (Bruker) at HKUST(GZ) Biosciences Central Research Facility (BioCRF). For total proteome analysis, the samples were analyzed in data-independent acquisition (DIA) mode, and the resulting data were processed using Spectronaut software for label-free quantification. For phosphoproteome analysis, the enriched phosphopeptides were analyzed in data-dependent acquisition (DDA) mode. The DDA data from the phosphoproteome were processed and analyzed using PEAKS Studio software for phosphopeptide and phosphosite identification.

Kinase prediction analyses

Kinase prediction analysis for DDX5 was performed using the PhosphoSitePlus Kinase Library tool (https://kinase-library.phosphosite.org/kinase-library/) (Johnson et al., 2023). All experimentally reported human DDX5 phosphopeptides listed in PhosphoSitePlus were extracted and individually submitted to the "Scan Substrate" module using default settings. For each phosphopeptide, the algorithm scores motif similarity against curated kinase recognition motifs and returns a ranked list of candidate kinases. Rankings for the top predicted kinases were recorded for each DDX5 phosphosite. Across multiple independent DDX5 phosphopeptides, CLK-family kinases (CLK1, CLK2, CLK3 and CLK4) consistently appeared among the highest-scoring motif matches, indicating that DDX5 contains sequence motifs compatible with CLK phosphorylation (Fig. S3).